To cite this version:

Approaches to Simulate Impact Damages on Aeronautical Composite Structures

R. P. LEMANLE SANGA[1,a)], C. GARNIER[1,b)] and O. PANTALÉ[1,c)]

[1]INP de Toulouse, ENI de Tarbes, Laboratoire Génie de Production, Université de Toulouse, avenue d'Azereix, B.P. 1629, 65016 Tarbes, France

[a] r.lemanle@enit.fr (corresponding author),
[b] christian.garnier@enit.fr,
[c] olivier.pantale@enit.fr

Abstract. Impact damage is one of the most critical aggressions for composite structures in aeronautical applications. Consequences of a high/low velocity and high/low energy impacts are very important to investigate. It is usually admitted that the most critical configuration is the Barely Visible Impact Damage (BVID), with impact energy of about 25 J, where some internal damages, invisible on the impacted surface of the specimen, drastically reduce the residual properties of the impacted material. In this work we highlight by the finite element simulation, the damage initiation and propagation process and the size of the defaults created by low velocity impact. Two approaches were developed: the first one is the layup technic and the second one is based on the cohesive element technic. Both technics show the plies damages by the Hashin's criteria. Moreover the second one gives the delamination damages with regards to the Benzeggah-Kenane criteria. The validation of these models is done by confrontation with some experimental results.

INTRODUCTION

Because of their high mechanical resistance and their lightness, composite materials are very much used in the aeronautic applications. However they are very sensitive to the damages caused by the aggressions induced by low velocity impact [1-3]. These damages are usually related to the rupture of fibers and matrix but also some delamination between the plies [4-6]. It is thus important to explore the damage mechanisms caused by these impacts. Numerical modeling by the finite element method is a powerful technic used to predict the behavior of some structure under dynamic solicitations. In this study we have used the Abaqus Explicit finite element code to simulate the evolution of the damage in a carbon fiber composite material as a result of a low velocity impact. We have chosen impact energy of 25 J which corresponds to the Barely Visible Impact Damage (BVID). Some recent studies using similar approaches have already been done published [7-9]. Within this field of investigation, there are two main approaches:

- The Layup approach giving the global behavior of the structure and the damages within the plies of the composite material. The limit of this technic is that it is not possible to compute damage along the thickness direction of the composite.
- The cohesive zone approach giving the damages within the plies, along the thickness direction and within the interfacial zone between plies. There is two ways to implement such an approach: the cohesive element technic and the cohesive surface technic.

In our approach we have used these three different approaches and have compared their results each other and with some experimental results.

1- EXPERIMENTAL APPROACH OF THE BVID IMPACT

1-1- Specimens used in experimental tests

Specimens used in this study are made from the composite epoxy RTM6 reinforced by carbon G0926 and have been produced by the liquid resin infusion process as reported in **Fig. 1**. The lay-up specimen is $\left[\left[\frac{0^o}{45^o}\right]_3\right]_S$ and the plate's size is $150 \times 100 \ mm^2$. Mechanical properties of the composite are given in **Tab. 1**.
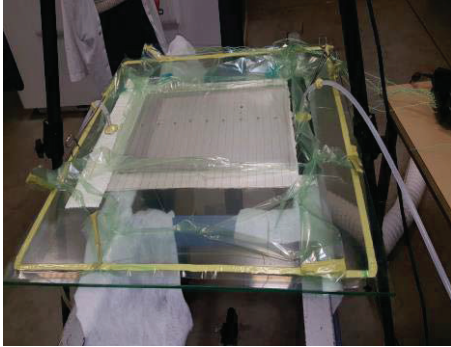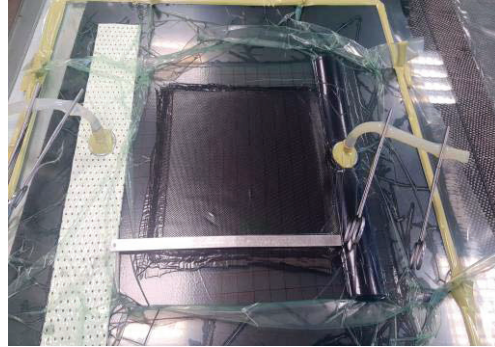
| (a) | (b) |

FIGURE 1. Manufacturing of composite specimen before (a) and after (b) the resin infusion

TABLE 1. Mechanical properties of the specimen

Young modulus	$E_1 = 67.9 \ GPa$	$E_2 = 67.9 \ GPa$	$E_3 = 12.1 \ GPa$
Shear modulus	$G_{12} = 6.2 \ GPa$	$G_{13} = 4.5 \ GPa$	$G_{23} = 4.5 \ GPa$
Poisson ratio	$v_{12} = 0.06$	$v_{13} = 0.17$	$v_{23} = 0.17$

1-2- Experimental device for impact tests

The impact tests were done with a MTT (Material Testing Technology) drop weight machine as illustrated in **Fig. 2** in conformity with the Standard ASTM D7136. This device has an impactor with a mass of 3 kg and a half sphere shape with a radius of R = 8 mm. The impact energy of 25 J is obtained by dropping the impactor from a total height of h = 0.85 m which confers to the impactor an impacting speed of 4.1 m/s.
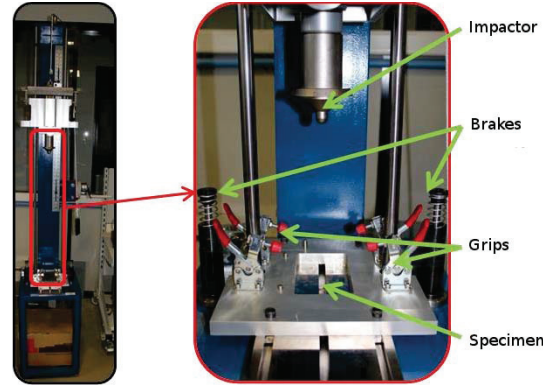
FIGURE 2. MTT drop weight machine

1-3- Analysis of the specimens after impact

The internal damage is evaluated using an infrared thermographic camera. The specimen is heated for 5 s and a 30 s movie is recorded with a frame-rate of 152 Hz. The presence of the defect appears during heating and cooling time and the output of this procedure is the projection of the internal default on a 2D plane as illustrated in **Fig. 3**. The measured surface of the defect has been evaluated to $449\ mm^2$.

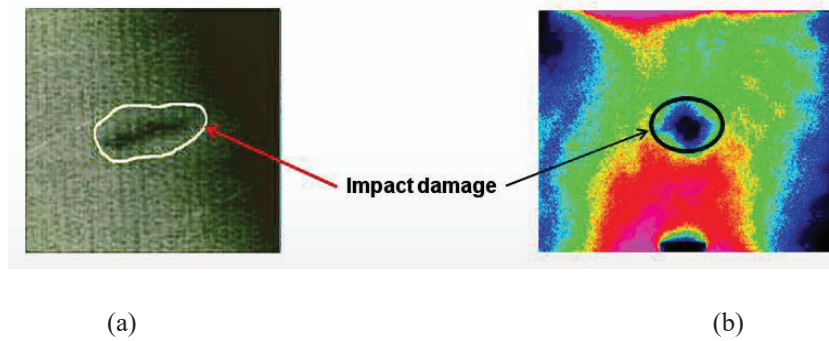(a)   (b)

FIGURE 3. Impact damage visualization by x-ray tomography (a) and infrared camera (b)

2- NUMERICAL SIMULATION OF THE BVID ON COMPOSITE

We have developed three different approaches: the first one is based on the layup technic and two other ones are based on the cohesive zone technic. These three approaches have been used within the framework of the Abaqus Explicit finite element code [10].

2-1- The layup approach

In this first approach, the composite structure is modeled by the S4R conventional shell finite element. This one is a 4 nodes quadrilateral conventional shell element with a reduced integration scheme. The Hashin [11] criteria are used here to simulate the initiation of damages.

Fiber tension $\hat{\sigma}_{11} \geq 0$: $\qquad F_f^t = \left(\dfrac{\hat{\sigma}_{11}}{X^t}\right)^2 + \alpha\left(\dfrac{\hat{\sigma}_{12}}{S^l}\right)^2$ $\qquad\qquad$ (1)

Fiber compression $\hat{\sigma}_{11} \leq 0$: $\qquad F_f^c = \left(\dfrac{\hat{\sigma}_{11}}{X^c}\right)^2$ $\qquad\qquad$ (2)

Matrix tension $\hat{\sigma}_{22} \geq 0$:

$$F_m^t = \left(\frac{\hat{\sigma}_{22}}{Y^t}\right)^2 + \left(\frac{\hat{\sigma}_{12}}{S^l}\right)^2 \qquad (3)$$

Matrix compression $\hat{\sigma}_{22} \leq 0$: $F_m^c = \left(\frac{\hat{\sigma}_{22}}{2S^t}\right)^2 + \frac{\hat{\sigma}_{22}}{Y^c}\left[\left(\frac{Y^c}{2S^t}\right)^2 - 1\right] + \left(\frac{\hat{\sigma}_{12}}{S^l}\right)^2 \qquad (4)$

where exponents $()^t$ and $()^c$ denote traction and compression respectively and indices $()_f$ and $()_m$ are used to refer to fiber and matrice respectively. Y^t and Y^c are the tensile and compressive strengths in the transverse direction, S^l and S^t are the longitudinal and transverse shear strengths respectively and α is a coefficient that determines the contribution of the shear stress to the fiber tensile initiation criterion. This later can be used to select the Hashin [11] model (where $\alpha = 1$) or the Hashin and Rotem [12] model (where $\alpha = 0$ and $S^t = \dfrac{Y^c}{2}$). The components of the effective stress tensor: $\hat{\sigma}_{11}$ (the stress in the fiber direction), $\hat{\sigma}_{22}$ (stress in the transverse-to-the fiber direction) and $\hat{\sigma}_{12}$ (in-plane shear fiber direction) are evaluated through the following relation:

$$\hat{\sigma} = \begin{bmatrix} \dfrac{1}{1-d_f} & 0 & 0 \\ 0 & \dfrac{1}{1-d_m} & 0 \\ 0 & 0 & \dfrac{1}{1-d_s} \end{bmatrix} \sigma \qquad (5)$$

where σ is the true stress and d_f , d_m and d_s are internal damage variables that characterize fiber, matrix and shear damages defined from the four damage variables: $d_f^t, d_f^c, d_m^t, d_m^c$ by the following relations:

$$d_f = \begin{cases} d_f^t & \text{if } \hat{\sigma}_{11} \geq 0 \\ d_f^c & \text{if } \hat{\sigma}_{11} \leq 0 \end{cases} \qquad (6)$$

$$d_m = \begin{cases} d_m^t & \text{if } \hat{\sigma}_{22} \geq 0 \\ d_m^c & \text{if } \hat{\sigma}_{22} \leq 0 \end{cases} \qquad (7)$$

$$d_s = 1 - (1-d_f^t)(1-d_f^c)(1-d_m^t)(1-d_m^c) \qquad (8)$$

At the beginning of the computation, we assume the following initial condition:

$$d_f^t = d_f^c = d_m^t = d_m^c = 0 \qquad (9)$$

Tab. 2 gives the different parameters defining the Hashin criterion.

TABLE 2. Damage properties of the specimen

Label	Variable	Stress (MPa)
Tension	$X^t = Y^t$	785
Compression	$X^c = Y^c$	612
Longitudinal shear	S^l	70
Transversal shear	S^t	55

2-2-   Cohesive zone approach

In the Abaqus finite element code, there is two ways to modelize the cohesive zone:

- The first one is the cohesive element approach. In this case all the 12 plies are meshed and linked one by one with 11 zero thickness cohesive plies giving a total of 23 plies. The composite plies are meshed on Abaqus by SC8R continuum shell elements and the cohesive plies are meshed using COH3D8 elements from the standard element library. The cohesive properties are assigned to the cohesive elements in the "Property" module of the Abaqus software.
- The second one, referred as cohesive surface, consists with the definition and the application of some cohesive properties between the plies in contact. For the Abaqus software, this assignation is done in the "Interaction" module.

The following equations define the traction separation formulation with quadratic stress and the Benseggagh-Kenane [13] criterion that were used to modelize the initiation and the propagation of damage within the cohesive zone. All the useful values are reported in **Tab. 3**.

$$\left(\frac{\langle\sigma_n\rangle}{N_{max}}\right)^2 + \left(\frac{\sigma_t}{T_{max}}\right)^2 + \left(\frac{\sigma_s}{S_{max}}\right)^2 = 1 \tag{10}$$

$$G_n^c + \left(G_s^c + G_n^c\right)\left(\frac{G_s + G_t}{G_s + G_t + G_n}\right)^\eta = G^c \tag{11}$$

Where $\langle\sigma_n\rangle = \frac{1}{2}\left(|\sigma_n| + \sigma_n\right)$

TABLE 3. Cohesive's mechanical and damage properties

Label	Variable	Value
Out of plane rigidity	K_{nn}	12265 Mpa
Shear rigidity	K_{ss}, K_{tt}	4530 MPa
Density	d	1.3
Out of plane tension resistance		75 MPa
Shear resistance		50 MPa
Mode I failure energy	G_n^c	800 $J.m^{-2}$
Mode II failure energy	G_t^c	1600 $J.m^{-2}$
Benzeggagh-Kenane coefficient	η	1.3
Tension failure energy	G_f^t, G_m^t	4820 $J.m^{-2}$
Compression failure energy	G_f^c, G_m^c	2930 $J.m^{-2}$

2-3-   Numerical simulation results

2-3-1-   The layup approach

- Assembled and meshed parts instances are:

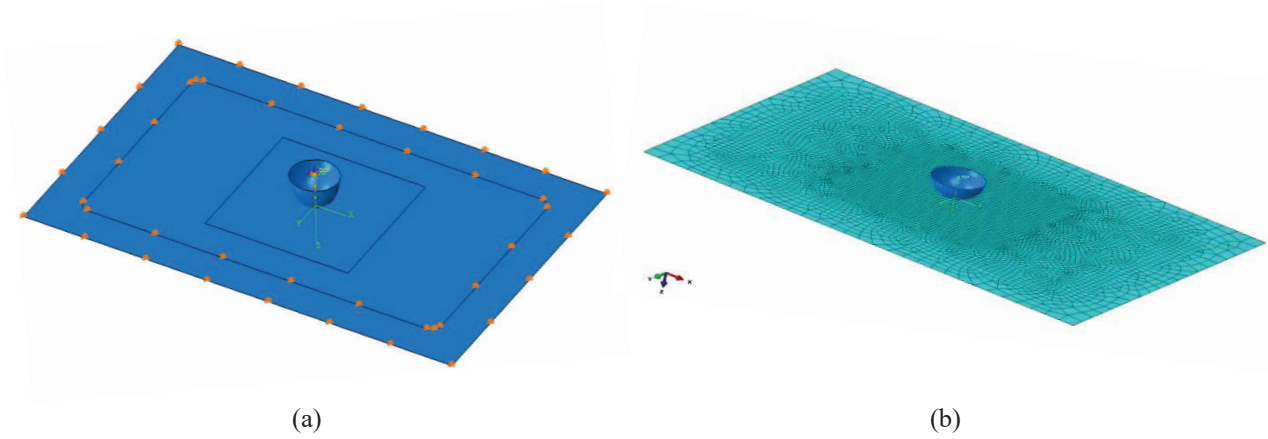(a)   (b)

FIGURE 4. Assembled (a) and meshed (b) part instances

The displacements were restricted by taking the pined boundary condition ($u_1 = u_2 = u_3 = 0$) for all nodes located along the lateral edges of the specimen in contact with the fixture base of the drop weight machine. The impactor is modelized as an analytical rigid, half hemispherical shell with a radius equal to $8\ mm$ and associated with a total mass of $3\ kg$.

- The Hashin damages are given in **Fig. 5**.

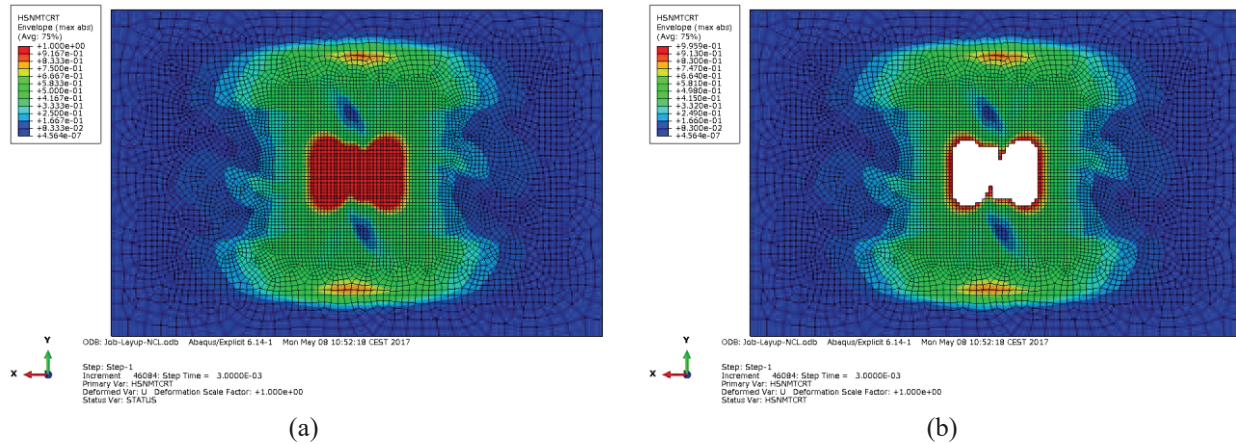(a)   (b)

FIGURE 5. The matrix Hashin damage (a). Damaged elements removed (b)

Fig. 5 shows the final matrix in traction damage with the Hashin criterion. The damage area is equal to 454 mm^2.

- Energies are given in the following graphs.

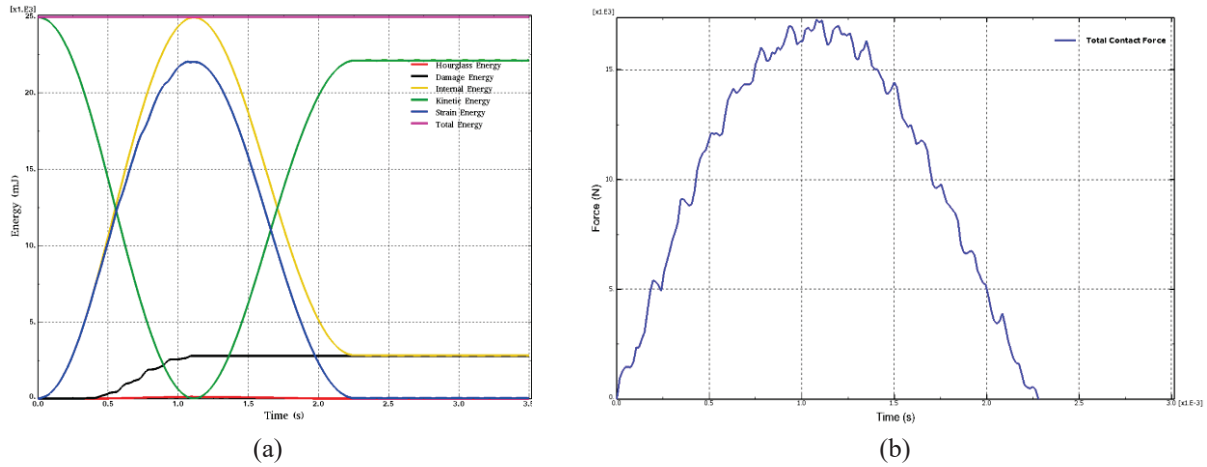(a)   (b)

FIGURE 6. Energies (a) and Total contact force (b)

Energies were plotted during the impact simulation. And we observe that the total energy remains constant. We also observe that the artificial Hourglass energy is very low at the end of the simulation. Finally we observe that the maximum deflection, the maximum contact force, the maximum damage and strain energy are obtained for time $t = 1.13\ ms$.

2-3-2-   Cohesive approach

- The plies and the meshed layers are given by:

As presented earlier for the layup approach, the same boundary conditions were used for the nodes located on the lateral edges in contact with the fixture base of the drop weight machine.
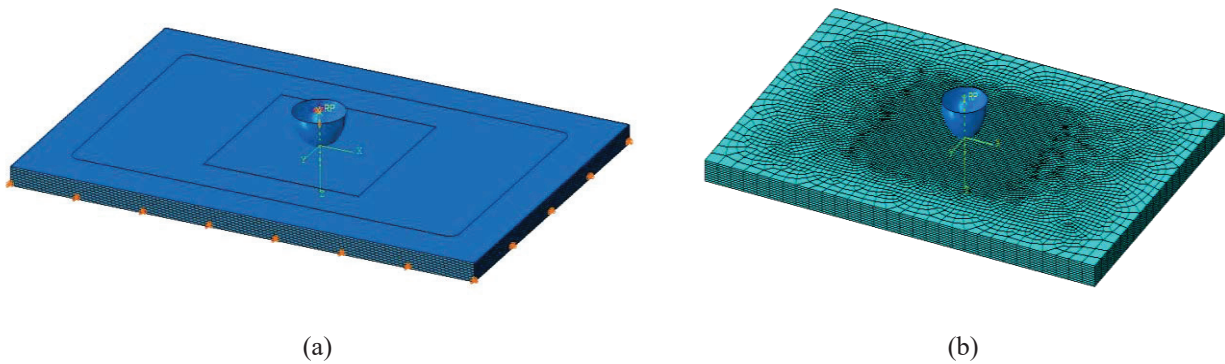

(a)   (b)

FIGURE 7. Assembled (a) and meshed (b) parts instances

- Cohesive element results are given in the following figures.
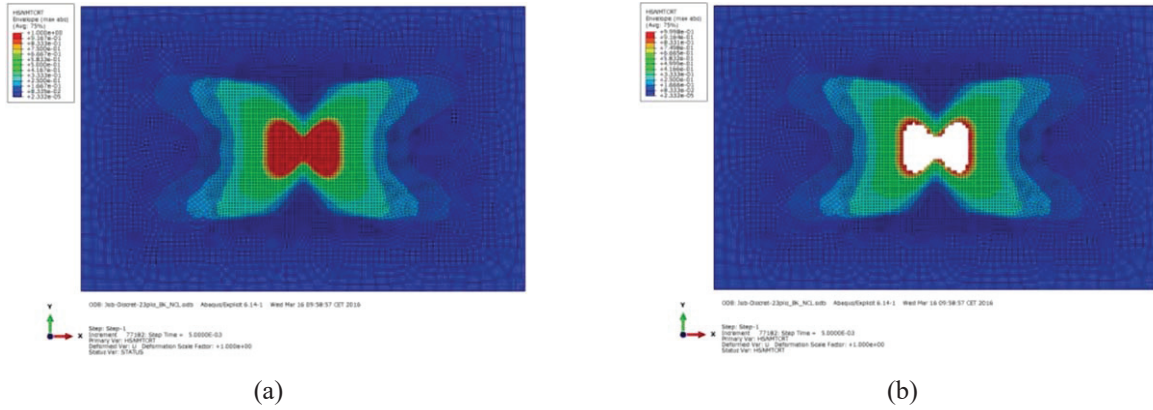
- Hashin's damages are given by:

(a)   (b)

FIGURE 8. The matrix Hashin damage on plies (a). Damaged elements removed (b)

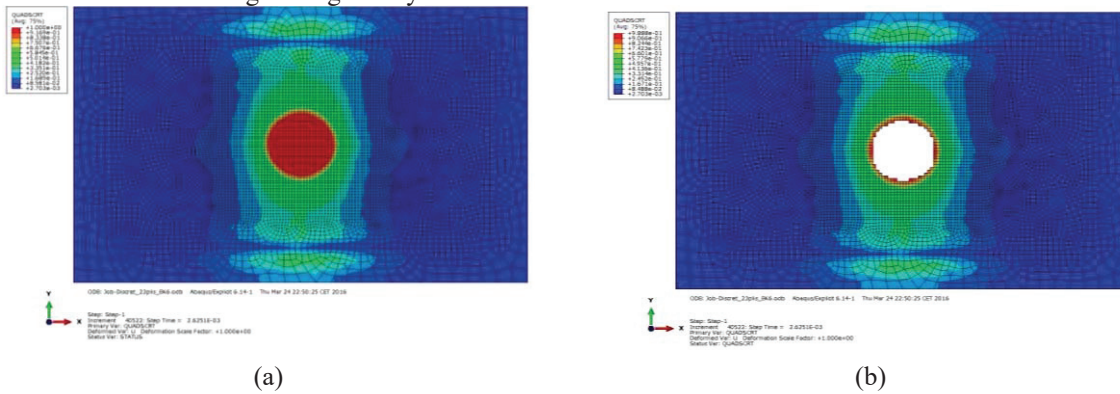- Interface's damages are given by:

(a)   (b)

FIGURE 9. Delamination damage on interfaces (a). Damaged elements remove (b)

The total matrix traction damage based on the Hashin criterion represents an area of $332\ mm^2$ while the delamination damage represents an area of $514\ mm^2$. The total damaged area is the superposition of the two previously defined areas. After an orthogonal projection, we can see that the matrix damage area is included in the delamination damage area. So we can conclude that the total damaged area given by the cohesive element approach is $514\ mm^2$.

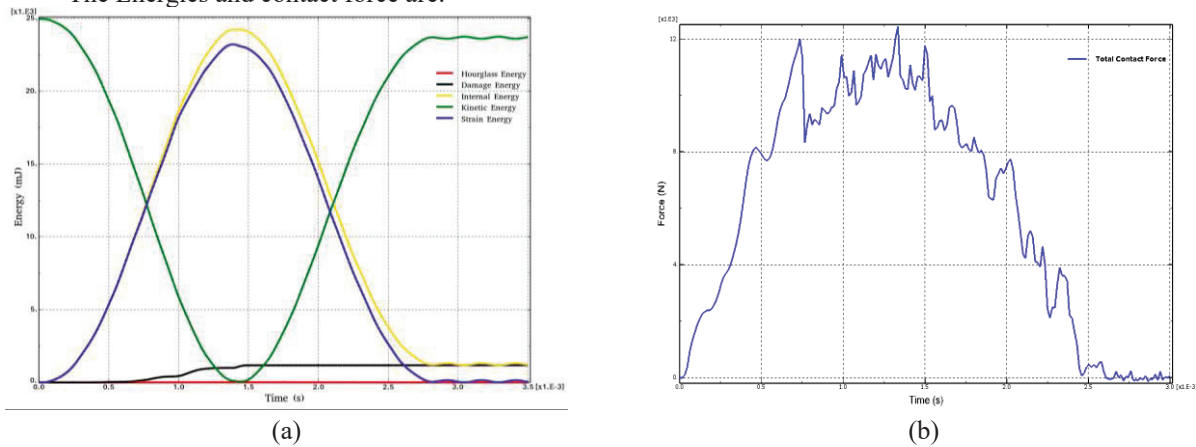- The Energies and contact force are:

(a)   (b)

FIGURE 10. Energies (a) and Total contact force (b)

Fig. 10. shows the evolution of the energies during the impact phase. As presented earlier, again, the hourglass energy remain very low during simulation.

- Cohesive surface result are given in the following figures
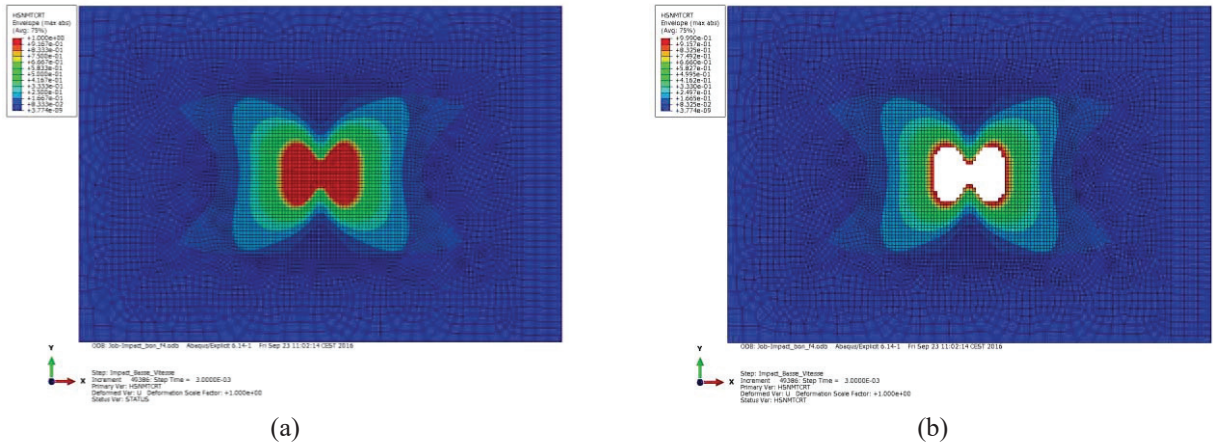
- Hashin's damages are given by:

(a)   (b)

FIGURE 11. The matrix Hashin damage on plies (a). Damaged elements remove (b)
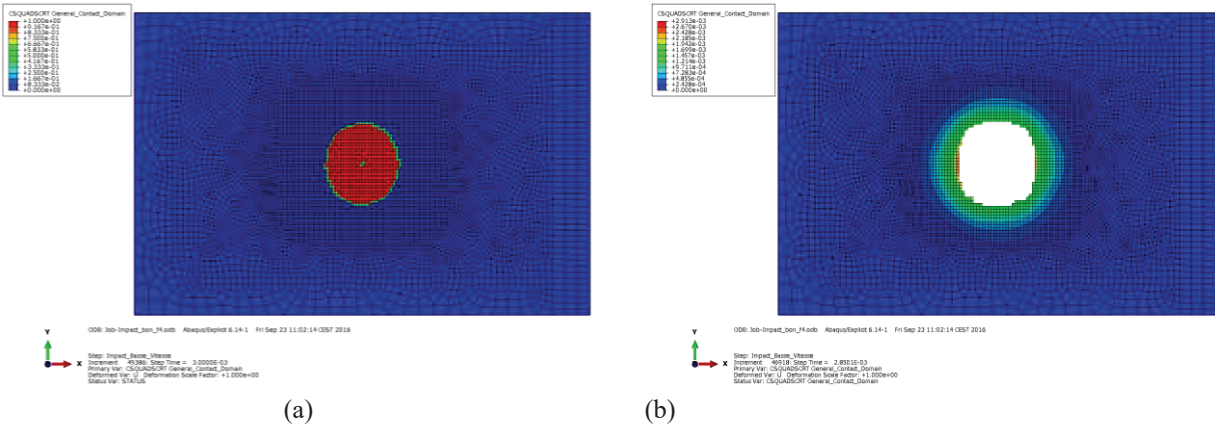
- Interface's damages are:

(a)   (b)

FIGURE 12. Delamination damage on interfaces (a). Damaged elements removed (b)

- Energies and total contact force are:
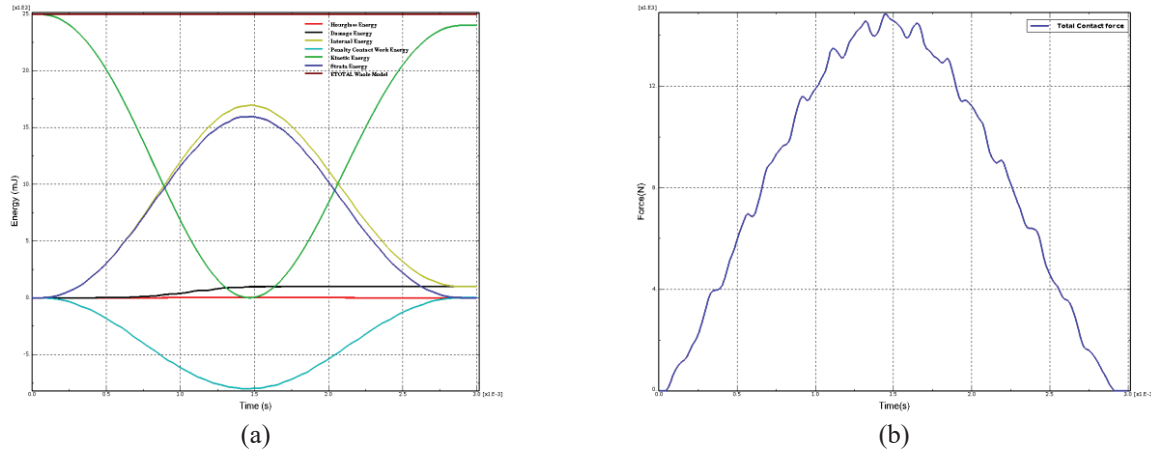
(a)   (b)

FIGURE 13. Energies (a) and Total contact force (b)

As in the cohesive element evaluation approach, we measured a total damage area of 461 mm^2 for the cohesive surface technic. The internal energy of the cohesive surface is very lower than the one of the cohesive element approach due to the energy absorbed as penalty work contact.

2-4- Analysis and discussion

A comparison of the computed damaged surfaces obtained with the numerical models and the experimental results shows that both models are in accordance. In fact, the experimentally measured damaged surface is more or less the minimal value because of the technology used for its evaluation. So the value obtained is not an absolute value because of the experimental protocol and the measurement error. Therefore, the difference given by both simulations can be considered inside of the error measurement. If the damaged area given by the layup is closer to the experimental result than those of the cohesive approaches, the cohesive approaches are more realistics, because they point out delamination damages. About computational time, the next table shows cpu-time for each of the three approaches for an impact step time of 3 ms on a HP Zbook PC with a RAM about 16 Gb and a processor Intel® Core™ i7-4810MQ CPU @ 2.80GHz ×8 on Ubuntu 15.04.

TABLE 4. Time duration

Model approach type	Time duration (s)
Layup	783
Cohesive element	8 414
Cohesive surface	22 118

CONCLUSION AND PERSPECTIVES

In this study we developed some models to simulate the BVID on a composite subjected to a low velocity and low energy impact. The finite element models we proposed in this paper are based on 3 different approaches: the layup, the cohesive elements and the cohesive surfaces. The validation of these models was done by comparison with some experimental results. The layup approach is a structural model, easy to implement while the cohesive

approaches are more realistic and more difficult to implement. They also involve much more computational time to complete. Further works concern the evaluation of the residual strength of the damaged composite plates by some compression after impact experiments. We also want to develop some numerical models to investigate the damages created by high velocity and high energy impacts. The final aim is to compare these damages on a panel of different energies and complete our knowledge about dynamic response of composite structures.

REFERENCE

1. F. Caputo, G. Lamanna, A. De Luca, V. Lopresto, *Numerical simulation of LVI test onto composite plates*, AIP Conf Proc, 1599, (2014), pp. 335–338.
2. G. Lamanna, R. Sepe, A. Pozzi, *Tensile testing of hybrid composite joints*, Appl Mech Mater, 575, (2014), pp. 452–456.
3. Z. Sharif-Khodaei, M. Ghajari, M.H. Aliabadi, *Determination of impact location on composite stiffened panels*, Smart Mater Struct, 21, (2012)
4. A.S. Kaddour, M.J. Hinton, P.A. Smith, and S. Li., *A comparison between the predictive capability of matrix cracking, damage and failure criteria for fibre reinforced composite laminates: Part a of the third world-wide failure exercise*. Journal of Composite Materials, 47(20-21), (2013), pp. 2749–2779
5. S. Abrate. *Impact on laminated composite materials*. Applied Mechanics Reviews, 44:155–190 (1991)
6. P. Chai, G.B. and Manikandan. *Low velocity impact response of fibre-metal laminates–a review*. Composite Structures, 107, (2014), pp. 363–381.
7. Lemanle Sanga, R.P., Garnier, C. and Pantalé, O., *Finite Element Simulation of Low Velocity Impact Damage on an Aeronautical Carbon Composite Structure*, Appl Compos Mater 23, (2016), pp. 1195.
8. F. Caputo, De Luca, R. Sepe, Numerical study of the structural behaviour of impacted composite laminates subjected to compression load, Composites Part B: Engineering 79, (2015), pp. 456–465
9. S. Jäger, A. Pickett, and P. Middendorf, *A discrete model for simulation of composites plate impact including coupled intra- and inter-ply failure.* Applied Composite Materials, (2016)
10. DS Simulia. The Abaqus v6.14 documentation collection, 2014.
11. Z. Hashin. *Failure criteria for unidirectional fiber composites*, Journal of applied mechanic, 47, (1980), pp. 329–334.
12. Z. Hashin and A. Rotem, *A fatigue criterion for fiber-reinforced materials*. Journal of Composite Materials, 7, (1973), pp. 448–464.
13. M.L. Benzeggagh and M. Kenane, *Measurement of mixed-mode delamination fracture toughness of unidirectional glass/epoxy composites with mixed-mode bending apparatus*, Composite Science and Technology, 56, (1996), pp. 439–449.